Composites Part B 167 (2019) 556–565

Contents lists available at ScienceDirect

Composites Part B

journal homepage: www.elsevier.com/locate/compositesb

New engineered stones: Development and characterization of mineral-glass composites

G.G. Santos*, M.C. Crovace, E.D. Zanotto

Department of Materials Engineering (DEMa), Center for Research, Technology and Education in Vitreous Materials (CeRTEV) Federal University of São Carlos (UFSCar), 13.565-905, São Carlos, SP, Brazil

ARTICLE INFO

Keywords:
Mineral surface
Composites
Glass-minerals
Sintering
Engineered stones

ABSTRACT

Engineered stones are high-end materials increasingly being used as kitchen countertops, floor and facade tiles, as well as in other architectural applications. These materials consist of approximately 70–95 wt% of mineral particles (usually quartz) dispersed in a matrix made of cement, ceramics or, much more often, polymer resins. Despite their very attractive aesthetic appeal, using polymer matrices is associated to low wear resistance, low chemical resistance and degradation by UV radiation or by contact with hot objects; therefore the use of a glass matrix can overcome some of these disadvantages. This paper addresses the development, optimization of compositions and thermal treatment of a novel type of composite - engineered stones - using recycled window glass and four distinct minerals. New glass-mineral composites were developed containing up to 70% weight of albite, alumina, petalite or quartz (the rest being window glass). The materials were characterized for their flexural strength, hardness, water absorption, thermal shock resistance and chemical durability. Except for the Quartz/glass composites, low-porosity materials (< 10%) with competitive properties if compared to commercial products were obtained. For instance, an Alumina/glass composite showed a (4-point) flexural strength of approximately 115 MPa and a hardness of 9 GPa, whereas commercial products (polymer and ceramic matrix) showed average values of 10 MPa and 70 GPa, respectively. The Petalite/glass composite exhibited high thermal shock resistance ($\Delta T_c \sim 330$ °C); whereas the Albite/glass composite showed very good chemical durability, with practically unchanged weight and visual aspect after coming into contact with both acidic and alkaline concentrated solutions. This new type of composite is thus very promising and warrants further study and development.

1. Introduction

Engineered stones, artificial marble, mineral surfaces or quartz surfaces are trade names for a type of synthetic tile that is widely used in decoration and construction as an alternative to natural stones, such as granite and marble. Their origin dates back to the 1960s in Italy, but they only became popular in Europe and North America in the 1990s. U.S. market reports (2013) showed that the market share of engineered stones were 7.9% [1], with an estimated annual growth of 7.4% [2].

Quartz powder is usually the main component in these materials due to its high hardness and chemical durability, availability and attractive price. Most commercial “surfaces” have about 90–94% by weight of quartz (or other mineral particles) connected by a matrix, which is usually made of polymer resin or cement [3].

Despite having positive characteristics, such as aesthetic appeal and durability, natural stones present increasing environmental problems in extraction, transportation and polishing processes, which may impair, delay or at least increase the cost of architectural projects [4]. Besides, merely as an example, it has been estimated that waste generated by extracting granite corresponds to about 25% of its total production [5]. Another problem lies in the environmental and social impacts caused by the activity in extraction areas [6].

On the other hand, the controlled processing by which engineered stones are produced makes them easier to install and allows a wide range of texture, design, color, size and shape. However, the most popular polymer matrix engineered stones have some disadvantages, such as: low scratch resistance, they are limited to indoor usage (to avoid UV degradation), and risk of permanent spotting when in contact with hot objects (above 150 °C) or by certain cleaning products.

Other types of engineered stones include cement or ceramic base matrices. The cement matrix type is the most accessible regarding price, but often presents high water absorption and inferior mechanical

* Corresponding author.
E-mail addresses: giseleguis@gmail.com (G.G. Santos), dedz@ufscar.br (E.D. Zanotto).

https://doi.org/10.1016/j.compositesb.2019.03.010
Received 30 October 2018; Received in revised form 13 February 2019; Accepted 3 March 2019
Available online 11 March 2019
1359-8368/

properties. In contrast, ceramic matrix engineered stones have excellent mechanical properties and durability, but the use of high processing temperatures significantly increase the product final price [7].

In this paper, we test and demonstrate the viability of using a recycled glass matrix as an alternative, novel type of engineered stone. A glass-mineral composite could in principle show attractive aesthetics, as well as good fracture strength, thermal shock resistance and chemical durability, and can also be used as external tiles, without the risk of UV degradation. Since glasses sinter at relatively low temperatures through viscous flow, the process cost could be significantly reduced compared to that of ceramic matrix composites. Moreover, the use of glass might lead to the formation of a natural surface glaze, which would work as an additional layer against water absorption.

For this task, in this study, several laboratory scale engineered stone samples containing four different minerals - albite, alumina, petalite and quartz - with recycled soda-lime-silica glass as the matrix were formulated and tested. It was demonstrated that a wide range of useful properties can be obtained, some having values comparable to those of commercial materials and others being even higher than those of competing natural stones.

2. Experimental

2.1. Selection and milling of raw materials

The glassy material used in our experiments was a recycled soda-lime-silica window glass due to its high availability, superior properties and low crystallization tendency during sintering. The minerals chosen were alumina (Alcoa, Poços de Caldas, Brazil), quartz (donated by Mineração Jundu, Descalvado, Brazil), petalite and albite (donated by Minérios Lorena, Lorena, Brazil), with average particle sizes ranging from 200 μm to 1 mm. These minerals were selected according to several factors and characteristics, such as being easy to handle, having different thermal expansion coefficients, which might affect the level of internal residual stress and overall fracture strength, and different hardness, which affects the scratch resistance of the composites.

Commercial soda-lime-silica glass plates were broken into smaller pieces with a diamond-tipped pen. These pieces were subjected to thermal shock (heating in a muffle furnace at 150 ± 7 °C for 10 min followed by immediate immersion in water at 20 ± 2 °C). Milling was performed first in a rotating disc mill (AMEF) with 1 mm of opening between the discs and then in a jet mill (Netzsch). Further millings were performed in a high impact planetary mill (Fritsch Pulverisette 6) with agate spheres of different sizes (10–30 mm) for 15–30 min with a rotational speed of 450–550 rpm, and alternating in clockwise and counter-clockwise directions to obtain a powder with particle size of 5–30 μm. The minerals were subjected to a similar milling process. The mixing of the materials was carried out in two stages: dry (physical mixing) followed by a wet (slip) step. The compositions used for all composites were set as follows (Table 1). The compositions were based on the same proportions of minerals and matrix of commercial materials.

2.2. Optical dilatometry

This was a particularly important first step since the sintering treatment parameters were chosen based on the results found by optical dilatometry. The optimum sintering temperatures of the composites were determined using an optical dilatometer (Misura HSM-ODHT 1600–8002, TA instruments), at a heating rate of 10 °C/min until 1300 °C, using manually pressed (25 MPa) pellets of 3.2 (diameter) x 4.5 mm (height). Once the sintering parameters (temperature and time) were optimized for all compositions, green bodies - 0.9 × 0.7 × 70 mm bars - were made in a hydraulic press (Carl Zeiss) and cold isostatic press (AIP CP360, American Isostatic Presses) at 100–200 MPa.

Table 1
Compositions utilized for initial optical dilatometry tests (wt%).

	Albite/glass	Alumina/glass	Petalite/glass	Quartz/glass
Comp. 1	95/5	95/5	95/5	90/10
Comp. 2	90/10	90/10	90/10	85/15
Comp. 3	85/15	85/15	85/15	75/25
Comp. 4	80/20	80/20	80/20	–
Comp. 5	75/25	75/25	75/25	–

2.3. Sintering treatments

The green bodies were placed into alumina sample holders, bathed in an alumina solution to avoid excessive adherence of the sintered surface. The sintering treatments were carried out in an electrical furnace (Keith, model KKSK 8.8 11–3000) equipped with a calibrated R-type thermocouple. The sintering treatment conditions were chosen according to the optical dilatometer results previously described.

2.4. Relative density, apparent porosity and water absorption tests

The sintered samples were evaluated regarding density and apparent porosity based on the standard ASTM C373-14a; they were kept at 150 °C ± 5 °C for a minimum of 24 h, cooled in a desiccator and weighed to determine the dry mass, D. The mass suspended in water, S, was measured by using a high precision balance (Mettler Toledo) equipped with a density determination kit. The samples were immersed in water for about 24 h and then taken out, dried lightly and weighed once again to determine M, the saturated wet mass of the samples. Calculations were made using the D, S and M values to determine open porosity, water absorption and bulk density (equations (1)–(3) below):

$$P = \frac{\frac{M-D}{V}}{100} \quad (1)$$

$$A = \frac{\frac{M-D}{D}}{100} \quad (2)$$

$$B = \frac{D}{V} \quad (3)$$

2.5. Mechanical properties

The next step consisted of determining some mechanical properties of the different samples, such as hardness and flexural strength. The hardness tests were performed in a Vickers' indenter (Future-Tech F-7). For the measurements, samples with dimensions of approximately 10 × 3 × 7 mm were cut and polished with 60, 80, 150, 240, 320, 400, 500, 600, 1200 grit silicon carbide papers and felt fabric with diamond pastes (Buehler) of 9, 6 and 1 μm particle size to obtain optical polishing. The indentations were performed based on ASTM C1327 - 08 - (Standard Test Method for Vickers Indentations).

The flexural strength tests were performed based on ASTM C 1161 - 02c (Standard Test Method for Flexural Strength of Advanced Ceramics at Ambient Temperature). The samples were submitted to four-point loading tests in a universal test machine (Instron). The results were compared between a group of samples with similar compositions and with commercial products.

2.6. Thermal shock resistance

The thermal shock resistance (based on ASTM C 1525–02 - Standard Test Method for Determination of Thermal Shock Resistance for Advanced Ceramics by Water Quenching) was determined by submitting the samples to three different temperatures (all above 150 °C) in a muffle furnace (EDG) for 30 min to ensure thermal equilibrium. The

samples were dropped into water at 23 °C (± 2) and then dried and tested for flexural strength (4-point tests). The results were compared to those found for samples not exposed to thermal shock. The critical temperature difference, ΔTc, or the temperature difference between the furnace and the water bath temperature that will cause a 30% drop in the average flexural strength, was estimated graphically. The aesthetics of the samples, such as color alterations, and the occurrence of cracks were evaluated by simple visual tests and microscopic analysis.

2.7. Chemical attack resistance

The chemical attack resistance (based on ASTM C650-04 - Standard Test Method for Resistance of Ceramic Tile to Chemical Substances) was determined by placing the samples (previously polished) in direct contact with acetic acid solution 10% v/v (Synth, 99,7%), citric acid solution 30 g/L (Synth, 99,5%) and sodium hydroxide 10% v/v (CHEMCO, 97%) for 24 h. Visual and pencil tests were conducted: the first consists of observing any signs of color alterations and stains, while the latter consists of making pencil marks in the region submitted to chemical attack and in the region that was not subjected to chemical attack. If the pencil mark could be erased equally from both regions, then the sample was labeled as “not affected”. Otherwise, the sample was considered as attacked. If the pencil mark cannot be removed in both areas, the pencil test does not apply.

2.8. Tribology tests

The compositions exhibiting the best set of properties for each composite were also investigated regarding the tribological behavior. The tests were performed in disc-shaped polished samples on a tribometer equipped with a tungsten carbide ball of approximately 6 mm in diameter. The following conditions were used during the tests: an applied force of 5 N, slip speed of 5 cm/s under normal atmospheric conditions (21 °C and 35% humidity); the coefficient of friction was continuously measured up to 10000 sliding cycles. The tests were performed in dry conditions. Measurements of topography and surface analysis were performed using an Asatan UNAT nanoindentator. The determination of the type of wear observed in the samples (abrasive, adhesive, etc.) was performed by scanning electron microscopy with field emission and X-ray spectroscopy by energy dispersion.

3. Results and discussion

3.1. Parameter optimization

In this work, our aim regarding parameter optimization (i.e., sintering temperature and duration of thermal treatment) was to keep the porosity of the composites at the lowest possible level. This was because pores have a great influence on the mechanical properties of any brittle material because they act as stress concentration points, promoting the propagation of cracks.

Fig. 1 illustrates dilatometric curves for different compositions of the mineral-glass composites studied, and Table 2 exhibits the sintering onset temperatures (i.e., the temperature at which the first alterations in the body dimensions occur). The amount of glass phase increased in the sequence from 1 to 5.

As shown in Table 2, it was not possible to measure the sintering temperature for the Quartz/glass composites due to the quartz phase transformations that take place in the working temperature range, a behavior that will be discussed later. The sintering temperature decreased with increasing the glass content (1–5) as expected, since glass sintering occurs through viscous flow.

Fig. 1 shows that Albite/glass composites have a sintering plateau near 1150 °C probably due to the albite melting, close to 1100 °C [8]. Since the glass is at or above it liquidus temperature, it can be said that the sintering stage for this composite occurs in a condition heavily influenced by the presence of a liquid phase.

The Alumina/glass composites exhibited a high onset sintering temperature (above 1350 °C) for all compositions. Higher sintering temperatures were expected for these composites due to the refractoriness of alumina, we believe that some kind of bond is formed at the interface between alumina and glass, which can cause an increase in the refractoriness of the latter. This strong bond was also referred to in previous works [9–11].

The Petalite/glass composites also exhibit plateaus for some compositions close to 1055 °C; but in this case, the plateaus correspond to the melting of the glass itself and become more prominent as more glass is added (Fig. 1, composition 3, 4 and 5). Because petalite has a high melting temperature (~1350 °C), the higher sinterability can be explained by the higher wettability of petalite particles by the glass.

As mentioned previously, the Quartz/glass composites show distinct dilatometric curves and it was not possible to pinpoint an onset sintering temperature, as the observed shrinkages are very low. A hypothesis is given below according to the three different regions in the dilatometric curve (Fig. 1):

1. Expansion (400 °C to 600 °C)

Quartz undergoes a notable phase transition where α-quartz becomes β-quartz (also called low-quartz ↔ high-quartz), occurring close to 570 °C which consists of a unit cell change from trigonal (α) to hexagonal (β) and 0.4% volume change [12].

2. Shrinkage (700 °C to 1000 °C)

Glass sintering occurs at nearly 700 °C and this fact might explain the shrinkage observed. However, the small shrinkage may occur due to the fact that part of the quartz particles are solubilized in the glass, which makes its viscosity increase.

3. Second expansion (above 1000 °C)

There is some uncertainty about this expansion. The quartz ↔ tridimite transformation occurs below 900 °C and the tridimite ↔ cristobalite transformation, above 1450 °C, indicating that the reason for this expansion must be a different one. Analyzing SEM micrographs, we have noticed the occurrence of what might be little circular crystals in the microstructure of Quartz/glass composites (Fig. 2). There is a possibility of the quartz particles act as nucleating agents for the glass, crystalizing phases, such as cristobalite and tridymite. The X-ray diffraction technique confirmed the presence of both phases (Fig. 3).

This behavior, as shown in Fig. 4, leads to a low shrinkage: the material still keeps 98% of its initial height after heat treatment at 1100 °C. This situation is problematic since the goal is to obtain high-density bodies, with at least 95% relative density. Low shrinkage means incomplete sintering and a high porosity in the final body.

3.2. Relative density, density, water absorption, total and apparent porosity

The best results obtained through optimized processes for each composition are shown in Table 3:

Table 3 shows that, with the exception of the Quartz/glass compositions, we obtained satisfactorily densified samples using the parameters and limits proposed in this work. The micrographs in Fig. 5 confirm this issue, i.e., while the composites of the other three minerals exhibit low porosity, the Quartz/glass microstructure is highly porous.

Fig. 6 shows optical microscopy micrographs of samples with different Quartz/glass proportions (ranging from 90–70 wt%); a high porosity persists.

The Quartz/glass composite micrographs (Fig. 6) and general properties data (Table 3) corroborate this problem as they exhibit highly porous surfaces, high open porosity, high water absorption and

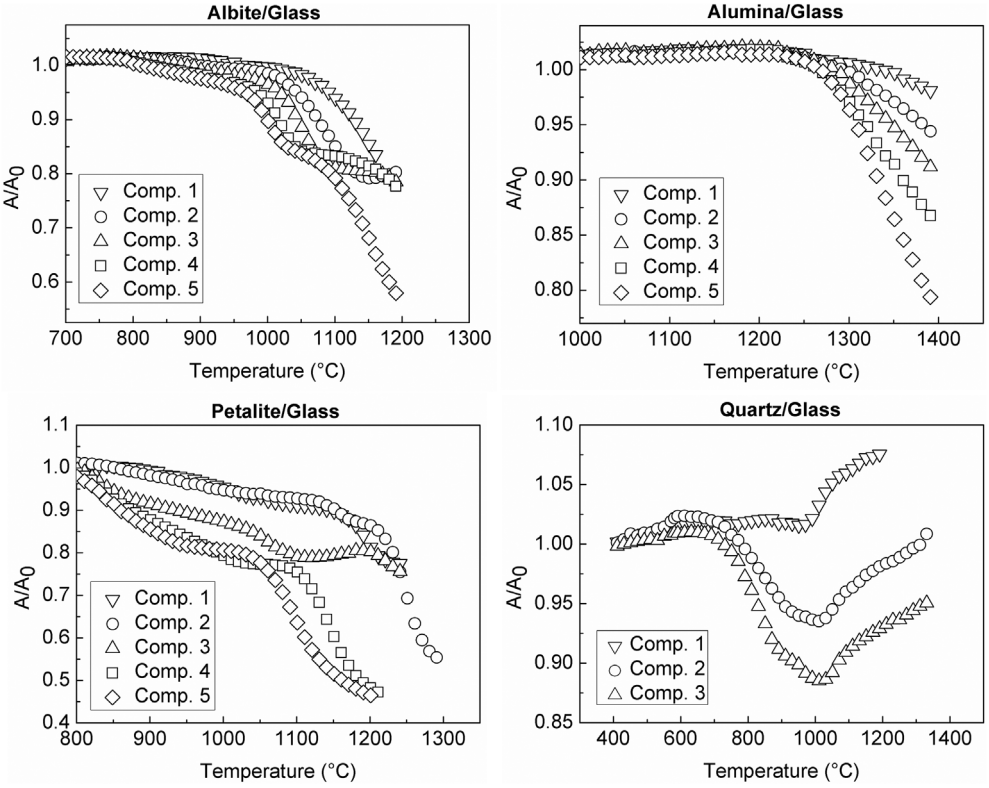

Fig. 1. Dilatometric curves of the compositions (Mineral/Glass).

Table 2
Sintering temperatures for the compositions shown in Fig. 1.

Compositions	Albite/glass	Alumina/glass	Petalite/glass	Quartz/glass
	Sintering Onset Temperature (°C)			
1	1125	–	1160	–
2	1070	–	1115	–
3	1045	1400	920	–
4	1015	1360	875	–
5	1000	1335	855	–

low relative density. We expected that an amount circa 20–40 wt% glass (the rest being quartz) would be enough to overcome some of these problems, since the glass could, in principle, flow through the material to fill in the pores, but our tests showed otherwise.

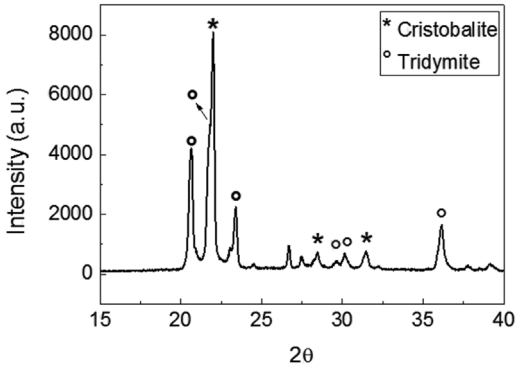

Fig. 3. X-ray diffratometer of Quartz/glass composite after sintering.

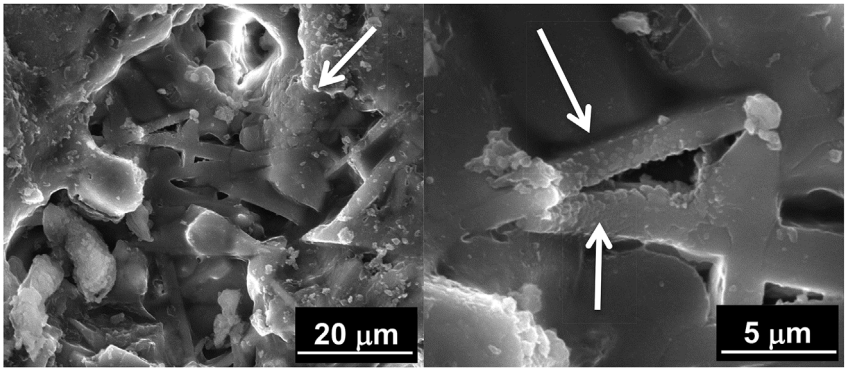

Fig. 2. SEM-micrographs of Quartz/glass composites. The arrows indicate the presence needle-like crystals at the interface between the glass and quartz particles.

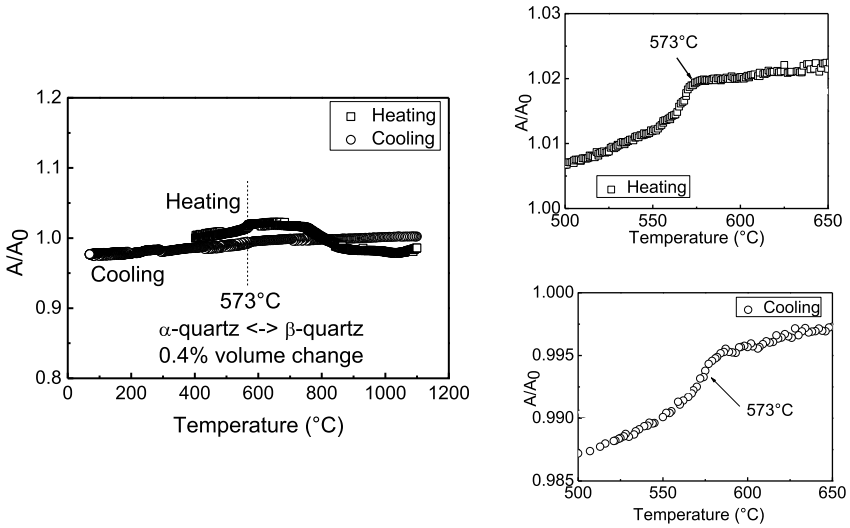

Fig. 4. Dilatometric curves for a sample containing 80% wt quartz (the rest is soda-lime-glass) in heating and cooling (left). The smaller graphs (right) show the α-quartz ↔ β-quartz transition in detail (heating and cooling).

3.3. Characterization

3.3.1. Hardness (Vickers)

Vickers tests were conducted to measure the hardness of the composites and the results are shown in Table 4:

The Hardness values were calculated by equation (4)

$$H_v = \alpha\left(\frac{P}{d^2}\right) \tag{4}$$

where P is the load, d is the indentation diagonal and α is a constant related to the geometry of the indenter (in this case, α = 1854).

3.3.2. Flexural strength: 4-point bending flexural tests

The compositions exhibiting lower porosity were tested for flexural strength in 4-point bending tests. The results are shown in Table 5, with the stress-strain curves in Fig. 7. The five first lines in Table 5 show values for commercial materials.

It is possible to estimate how much the porosity influenced the flexural strength values by equation (5) [19]:

$$S = S_0 \exp(-nP) \tag{5}$$

where, S = flexural strength, S_0 = estimated flexural strength of a fully densified material, n = constant from 4 to 7, and P = porosity (< 1).

Using the data in Table 3 for porosity (P), the data in Table 5 for flexural strength (S), and the average value of 5.5 for n, S_0 can be determined for all the compositions studied in the 4-point bending flexural tests (Table 6):

The data from Table 6 are shown in a bar chart for better visualization (Fig. 8):

As shown in Fig. 8, the most discrepant value between S and S_0 is the that for the quartz/glass composite, as expected. The estimated flexural strength of a fully densified body (S_0) is about 145 MPa (Table 6), however the S value found in our measurements was not more than 18 MPa, which is a meaningful reduction.

The Alumina/glass composite exhibited the best set of mechanical properties; their hardness is similar to values of ceramic matrix engineered stones [15]. Furthermore, the flexural strength of this composite is twice as high as those of common commercial products [15]. The Albite/glass composite exhibited good mechanical properties compared to the commercial products as well: not as high as the ones found in the Alumina/glass composite, but quite competitive.

The Petalite/glass composite, although having good hardness, exhibited considerably low flexural strength compared to the other compositions in this work (except the Quartz/glass composite). According to Fig. 8, the porosity of the Petalite/glass composite was not the only factor affecting the flexural strength value, especially comparing it to the other compositions. Alumina/glass and Quartz/glass showed a 42% and 81% of a difference between S and S_0, respectively, while Petalite/glass exhibited “only” a 25% difference.

This relatively small strength is probably related to a significant thermal expansion coefficient difference between the two existing phases: soda lime silica glass ($\sim 10 \times 10^{-6}\,K^{-1}$) and petalite ($\sim$0,5–1x$10^{-6}\,K^{-1}$) [20]. The residual stress in the matrix, σ, can be estimated through the Hsueh and Becher equation [21], based on the Eshelby model [22] for spherical inclusions (Equation (6)).

$$\sigma_{11} = \sigma_{22} = \sigma_{33} = \frac{(\alpha_m - \alpha_e).\ \Delta T}{\frac{1}{3K_e} + \frac{1}{4(1-f)G_m} + \frac{f}{3(1-f)K_m}} \tag{6}$$

where: α = thermal expansion coefficient, ΔT = range of temperatures at which internal stresses develop, K = bulk modulus, G = shear modulus, f = fraction of inclusions, e = subscript that refers to inclusions, m = subscript that relates to the matrix.

The estimated values for each composition are shown in Table 7:

The largest residual stress is exactly that of the Petalite/glass composite. Considering petalite as the matrix (because it can be found in a larger quantity), the matrix is being submitted to large tensile stress

Table 3
Water absorption, apparent porosity, bulk density and relative density for the studied compositions.

Compositions/Properties	Albite/glass	Alumina/\glass	Petalite/glass	Quartz/glass
Water absorption (%)	< 1	< 1	< 1	12 ± 1
Apparent Porosity (%)	< 1	< 1	< 1	20 ± 1
Total Porosity (%)	4	10	5	–
Density (g/cm^3)	2.44 ± 0.01	3.19 ± 0.04	2.29 ± 0.01	1.63 ± 0.02
Relative Density (%)	95	89	94	63

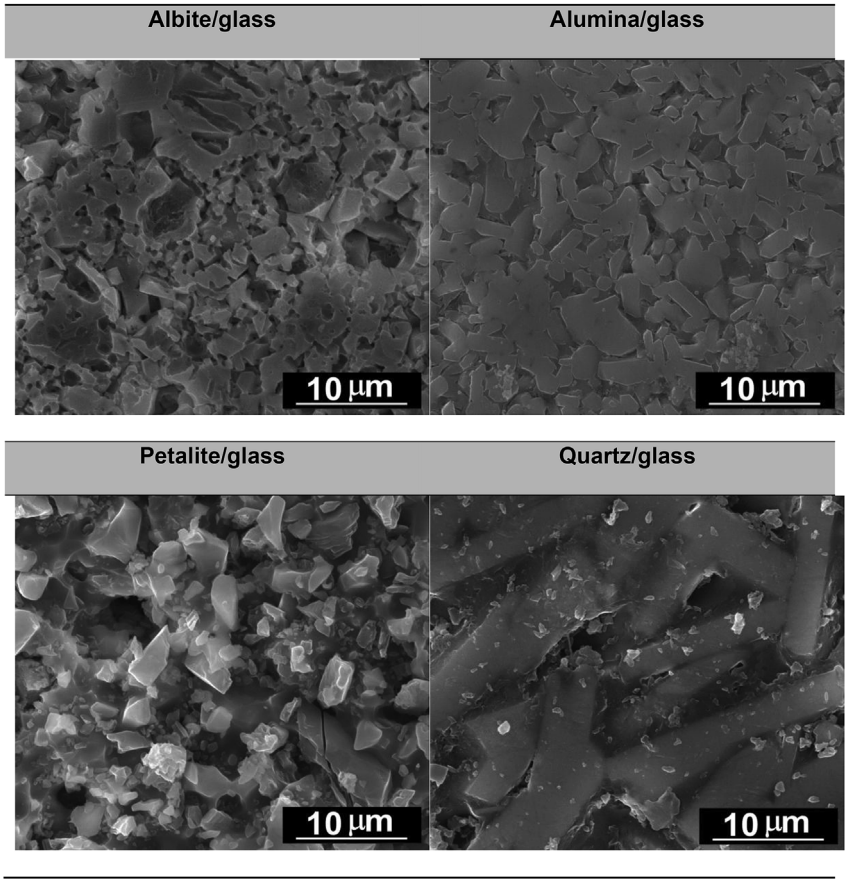

Fig. 5. Scanning electron microscopy micrographs of the compositions obtained through optimized conditions. The samples were etched with a concentrated solution of hydrofluoric acid to reveal the microstructures.

(positive sign, by convention) and it can be one of the factors influencing the flexural strength of this composition. It is worth noticing, however, that the flexural strength of the Petalite/glass composite is similar to that of some granites, marbles and engineered stones with cement matrix. Combining these aspects with the low water absorption and low open porosity, the Petalite/glass composite still could be used as engineered stone.

Finally, let us discuss the lower flexural strength value of the Quartz/glass composite. In this case, three factors might be responsible: (1) high porosity due to incomplete sintering, (2) the compressive stress

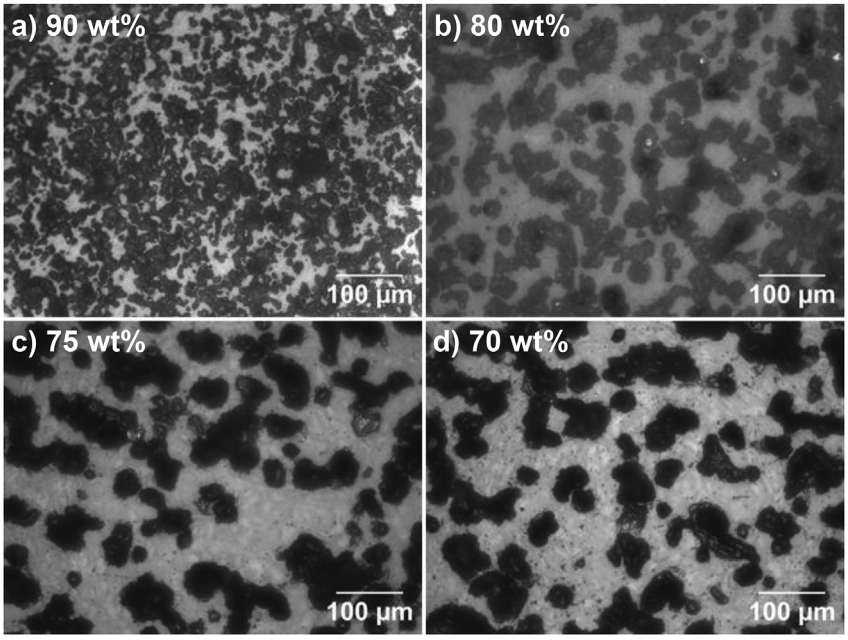

Fig. 6. Micrographs of Quartz/glass samples containing 90–70 wt% of glass. The amount of glass increases from left to right and from top to bottom.

Table 4
Hardness of the composites developed in this study and characteristic values for commercial materials.

Composition/Material	Hardness (GPa)
Engineered Stone (polymer matrix)	*9* [13]
Marble	*3-5* [14]
Granite	*8-11* [14]
Albite/glass	8.2 ± 0.3
Alumina/glass	9.8 ± 0.4
Petalite/glass	8.6 ± 0.8

Table 5
Compositions and values of flexural strength and average value for commercial products for comparison.

Composition/Material	4-point Flexural strength (MPa)
Engineered Stone (ceramic matrix)	*59-67* [15]
Engineered Stone (cement matrix)	*8-12* [16]
Engineered Stone (polymer matrix)	*28-79* [13]
Marble	*15* [17]
Granite	*11* [18]
Albite/glass	57 ± 2
Alumina/glass	115 ± 2
Petalite/glass	39 ± 1
Quartz/glass	18 ± 2

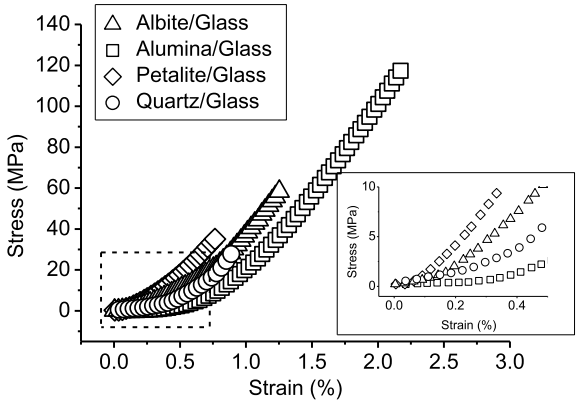

Fig. 7. Stress-strain curves for the studied compositions.

Table 6
Estimated values of the flexural strength of a fully densified body, S_0.

Composition	S_0 (MPa)	Reduction in S compared with Table 5 (%)
Albite/glass	74	23
Alumina/glass	199	42
Petalite/glass	52	25
Quartz/glass	145	81

to which the matrix is being subjected (negative sign) and (3) the presence of cracks due to the difference in the thermal expansion coefficient between quartz and which rise up during cooling and are accentuated by the phase transformation quartz taking placeing about 570 °C.

3.3.3. Thermal shock resistance

A material used on kitchen countertops and as external tiles should ideally have high resistance to thermal shock - sudden changes in temperature. Samples of Albite/glass, Alumina/glass and Petalite/glass were tested according to the NBR 31818–1997 and ASTM C1525-02 standards. Due to its higher porosity, the Quartz/glass samples were not tested. The thermal shock temperatures were chosen based on previous

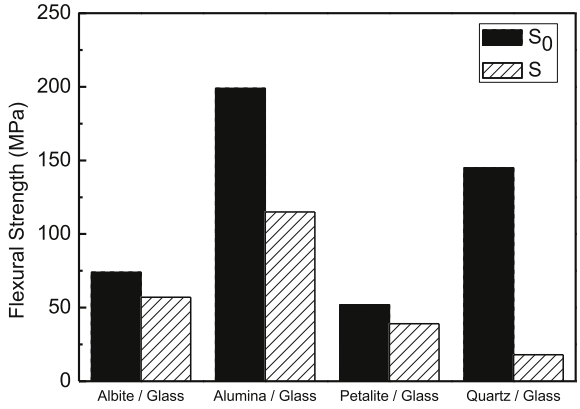

Fig. 8. Bar chart comparing the S_0 and S values for the studied compositions.

Table 7
Estimated residual stress values for each composite according to Equation (6) (considering cooling from the sintering temperature).

Composition	Estimated residual stress at the matrix (MPa)
Albite/glass	26
Alumina/glass	140
Petalite/glass	454
Quartz/glass	−65

works [23,24]. After each thermal shock, the samples were evaluated regarding their flexural strength, and the data were compared with the flexural strength values obtained for samples that were not submitted to thermal shock (Table 5 and Fig. 7). The critical temperature difference, ΔT_c, was estimated graphically, however it is recommended using the material at temperatures immediately below that responsible for 30% decrease in flexural strength. The results are shown in Table 8 and Figs. 9–11:

The three tested compositions exhibited good flexural strength even when submitted to a sudden change of temperature. It is important to notice the evolution of the flexural strength as the thermal shock temperatures increases. The Albite/glass composition exhibits the most marked drop in flexural strength. Undoubtedly, the Petalite/glass composite shows the best results, with consistent flexural strength values even when submitted to thermal shocks in the temperature range of 150–300 °C. Its critical temperature difference, ΔT_c, is also the highest among all the compositions, 330 °C.

Moreover, the samples remained visually the same after thermal shock at temperatures below 150 °C, without the appearance of cracks or stains. This is a good result that complies with ASTM C484 (2014) that suggests a temperature of 145 ± 5 °C for the visual test.

For the second and third thermal shock temperatures, all compositions exhibited a decrease in flexural strength. The most notable one was for the Albite/glass composite (Fig. 9). The critical temperature difference, ΔT_c, namely the temperature difference that leads to a flexural strength drop of 70%, was approximately 180 °C. In addition, above this temperature, at 220 °C, some small cracks could be seen on the material surface (Fig. 12).

The Alumina/glass composite exhibited a decrease of 12% in the first thermal shock temperature (200 °C) and a reduction of 65% in the flexural strength after thermal shock at 300 °C (Fig. 10 and Table 8). In other words, in a 100 °C temperature range, the flexural strength reduction was approximately 50%. Although the decrease is quite significant, it is worth noting the high temperatures from which these thermal shock experiments were performed (200 and 300 °C). Finally, it is unlikely that this type of composite will be used in any application that requires temperatures above 200 °C.

The best thermal shock resistance was shown by the Petalite/glass

Table 8
Thermal shock temperatures and flexural strength of the Albite/glass, Alumina/glass and Petalite/glass composites.

Comp.	Temp.1 (°C)	Flexural strength (MPa)	Temp.2 (°C)	Flexural strength (MPa)	Temp.3 (°C)	Flexural strength (MPa)
Albite/Glass	150	55 ± 5	180	34 ± 2	220	9 ± 1
Alumina/Glass	200	94 ± 19	300	41 ± 1	400	34 ± 5
Petalite/Glass	150	35 ± 2	300	31 ± 3	450	14 ± 2

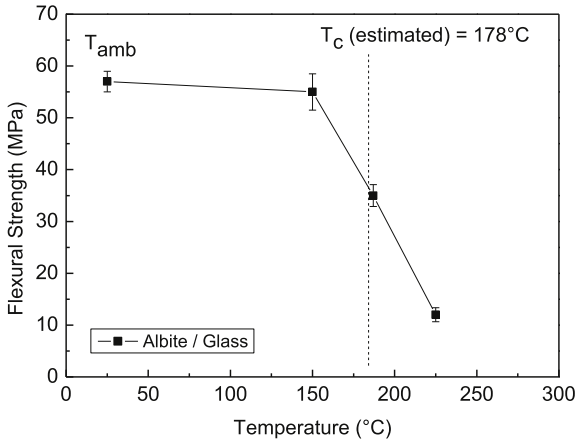

Fig. 9. Flexural strength evolution of the Albite/glass composite. Tests conducted at room temperature, after 150 °C thermal shock, after 180 °C thermal shock and after 220 °C thermal shock. Maximum recommended use temperature: 150 °C.

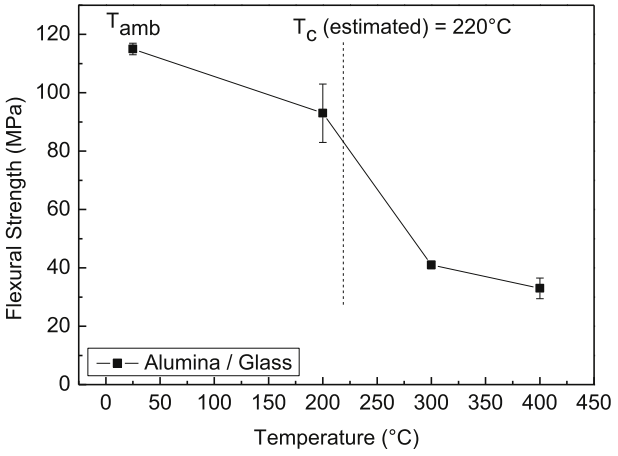

Fig. 10. Flexural strength evolution of the Alumina/glass composite. Tests conducted at room temperature, after 200 °C thermal shock, after 300 °C thermal shock and after 400 °C thermal shock. Maximum recommended use temperature: 200 °C.

composite. This result was already expected as petalite is a mineral of the lithium alumina silicate group (LAS), materials that are largely used in applications that require high thermal shock resistance, such as cooktop plates and microscope mirrors [25]. This class of materials presents extremely low thermal expansion coefficients, which may even be negative for some phases, depending on the crystalline direction [25]. Fig. 11 and Table 8 show that the first thermal shock temperature (150 °C) provided a 10% decrease in the flexural strength value while the second temperature (300 °C), a 20% reduction. In other words, an increase of 150 °C in the thermal shock temperature generated only a 10% reduction in flexural strength. The third thermal shock temperature (450 °C) caused a significant decrease in flexural strength: 65% compared to the initial value. The T_c estimated according to Fig. 11 is 330 °C, a temperature that is certainly above the maximum range needed for a material to be used as engineered stone.

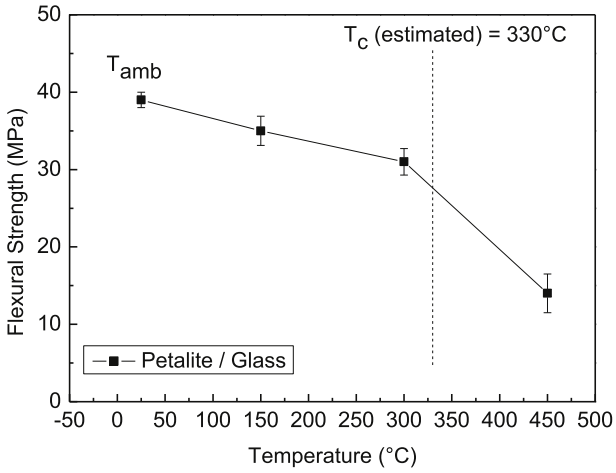

Fig. 11. Flexural strength evolution of the Petalite/glass composite. Tests conducted at room temperature, after 150 °C thermal shock, after 300 °C thermal shock and after 450 °C thermal shock. Maximum recommended use temperature: 300 °C.

3.3.4. Resistance to chemical attack

The Albite/glass, Alumina/glass and Petalite/glass composites were submitted to 24 h of chemical attack tests with the following substances: acetic acid (10% v/v), citric acid (30 g/L) and sodium hydroxide (10% v/v). Following these tests, visual and pencil tests were conducted. The Alumina/glass sample was the only one to show visible differences after the chemical attack test; the sample started to show a light yellow color on the part of the surface submitted to direct contact with all the solutions used.

Table 9 shows the results of the pencil test for samples submitted to 24 h of contact with solutions of acetic acid, citric acid, and sodium hydroxide:

As can be seen in Table 9, it was not possible to completely erase the pencil mark only for the Alumina/glass composite. The corrosion mechanism of sintered alumina has been extensively studied and it is related to the dissolution of grain boundary impurities, such as MgO and Fe_2O_3 [26]. However, the result of this study is probably a direct consequence of the high porosity exhibited by this sample after polishing. In addition, even without polishing, the surface of the Alumina/glass samples is rougher than that of the Albite/glass and Petalite/glass composites and is easily stained if in contact with a dusty surface, for example. The glazed layer, observed in samples of Albite/glass and Petalite/glass is not as significant in the Alumina/glass composites.

The Albite/glass and Petalite/glass composites exhibited good resistance to chemical attack by acetic acid (10% v/v), citric acid (30 g/L) and sodium hydroxide (10% v/v). The samples kept the same visual aspects (such as surface integrity and gloss) before and after the tests, as well as the same weight. Furthermore, the two mentioned composites showed good results in the pencil test, being labeled as “not affected” by the chemical attack tests (Figures from Table 9).

However, the same cannot be said about the Alumina/glass composites. All samples exhibited a yellowish tone after the tests, regardless of the substance with which they were in contact. In addition, the pencil scratches could not be completely erased in any of the sample areas (the area tested and the area not subjected to the test, Table 9), which

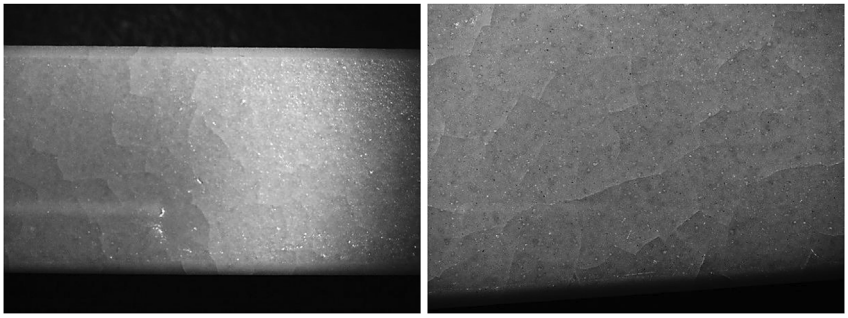

Fig. 12. Cracks on the surface of the Albite/glass composite after thermal shock at 220 °C.

Table 9
Samples subjected to chemical attack tests.

Comp.	Status	Acetic acid (10% v/v)	Citric acid (30 g/L)	Sodium hydroxide (10% v/v)
Albite/glass	Pre-test	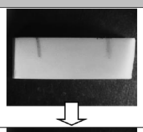	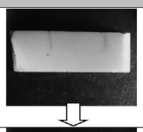	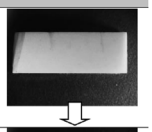
	After-test		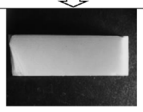	
Alumina/glass	Pre-test	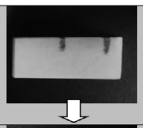	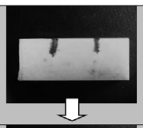	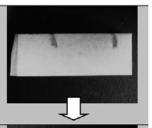
	After-test	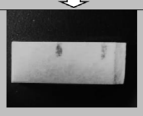	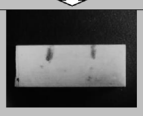	
Petalite/glass	Pre-test	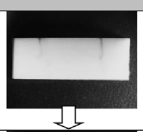	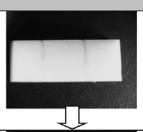	
	After-test	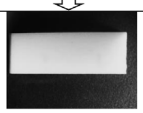		

indicates that the pencil test does not apply in this case. It was previously noticed that the Alumina/glass composite exhibited a highly porous surface after polishing, and was easily stained by external factors. One solution for this problem can be the use of a glaze acting as an additional layer against stains and particles, but no test was made to evaluate this solution. It is worth noting that granites might also have a highly porous surface, but since they are usually dark, dirt and stains are not typically visible on their surfaces, and they are visually unchanged for a long period of time.

3.4. Tribological properties

The friction coefficient, W, and the wear rate of Albite/glass and Petalite/glass samples were determined by pin-on-disk tests. To clarify, the maximum applied force of the equipment, 10 N, was not enough to generate impressions in the Alumina/glass composites; therefore, their results are not reported here. Fig. 13 shows the coefficient of friction of

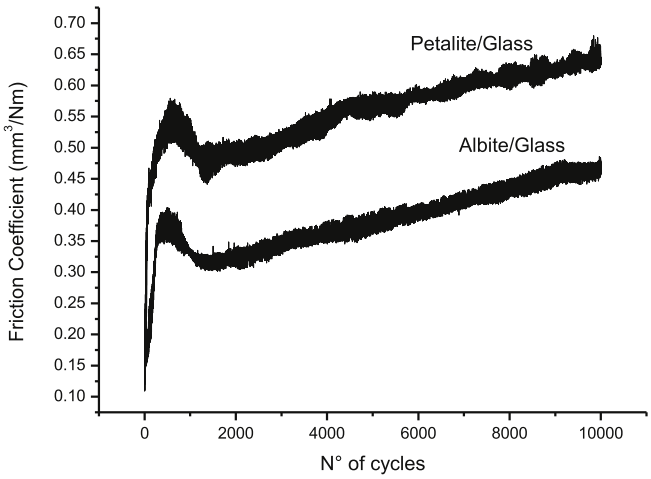

Fig. 13. Friction coefficient as a function of the number of cycles of samples of Albite/glass and Petalite/glass.

Table 10
Friction Coefficient and wear rate of the Albite/glass and Petalite/glass composites.

Composite	Friction Coefficient	Wear Rate ($\times 10^{-6}$ mm^{-3}/Nm)
Albite/glass	0.38 ± 0.01	1.94 ± 0.39
Petalite/glass	0.57 ± 0.01	3.69 ± 1.31

the samples as a function of the number of cycles, while Table 10 shows the values of friction coefficient and wear rate:

The friction coefficient, W (Equation (7)), was determined for the steady-state and dry surface conditions.

$$W = \frac{V}{PL} \tag{7}$$

where: P = applied load, L = sliding distance, V = calculated volume assuming an elliptical wear profile, which can be given by Equation (8):

$$V = \frac{\pi whl}{2} \tag{8}$$

where w is the wear groove width, h is the wear groove depth and l is the wear track length.

Table 10 shows that the value of W is higher for the Petalite/glass composite than for the Albite/glass composite. The friction coefficient measured in the pin-on-disk tests is dynamic and it is known that the higher its value, the greater the resistance to slipping. An important fact is that the coefficient of friction for commercial products with ceramic matrix is 0.77–0.80. However, the values obtained in this study are similar to the values obtained by Buchner et al. [27] for black granite and porcelain stoneware commonly used. The authors reported

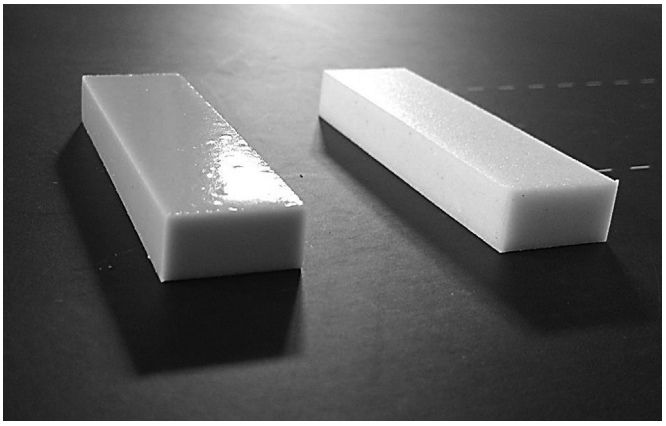

Fig. 14. Visual of the composites containing Albite/glass (left) and Petalite/glass (right). The dimensions of the samples are approximately 9 × 18 × 60mm.

coefficient of friction values of 0.44 and 0.54 for black granite and the porcelain tile tested, respectively.

3.5. Visual aspects of the sintered material

Fig. 14 shows two samples of the material developed in this work immediately after sintering treatments. It can be seen that both have a glossy surface naturally, without the process of polishing. The Alumina/glass composite, not shown here, is also white but with a more opaque aspect in the surface.

4. Conclusions

Except for the Quartz/glass composite, all the other developed engineered stones in this work exhibit a set of characteristics recommended for construction tiles and kitchen countertops. The Quartz/glass composites exhibited the lowest sinterability, even for compositions with high (20–30 wt%) glass content. Besides the high porosity, the α-quartz ↔ β-quartz phase transition contributed to the reduction of strength, because of the significant volume changes that cracks the material on the cooling path after sintering.

The other three composites have low porosity, low water absorption, superior chemical durability, high hardness, useful flexural strength, and good thermal shock resistance. The Alumina/glass and Albite/glass composites exhibited the best set of mechanical properties, especially the first, with an average flexural strength of 115 MPa. However, this composition does not have the best chemical attack resistance against acids. The Petalite/glass composite shows a very good performance in thermal shock tests, with a critical temperature around 330 °C. However, overall, the Albite/glass composite exhibited the most balanced set of properties.

Therefore, this novel type of glass matrix *engineered stone,* with the innovative use of a recycled glass matrix, shows competitive properties compared to natural and synthetic commercial materials and warrants further study and development towards large scale production.

Acknowledgments

The authors would like to thank Prof. Francisco C. Serbena and Crislaine Cruz from the Federal University of Ponta Grossa (UFPG) for the tribological tests. The authors thank the Laboratory of Structural Characterization (LCE/DEMa/UFSCar) for the general facilities. We are also grateful to the Brazilian mineral companies, Mineração Jundu for donating the quartz sand, and Minérios Lorena for the petalite and albite. We are also grateful to FAPESP – the São Paulo Research Foundation (Process no. 2013/07793–6), CNPq – National Council for Scientific and Technological Development (Process no. 141457/2013–9) and CAPES (Coordination for the Improvement of Higher Education Personnel) for their financial support of this research.

References

[1] U.S.. Countertop market annual growth: 4.2%. Stone update. 2015http://www.stoneupdate.com/news-info/latest-stuff/930-u-s-countertop-market-annual-growth-4-2, Accessed date: 4 July 2018.
[2] U.S. Natural-Stone. Countertop demand growing. 2013 Stone Update http://www.stoneupdate.com/news-info/latest-stuff/592-us-natural-stone-countertop-demand-growing, Accessed date: 4 September 2018.
[3] Lam dos Santos JP, Rosa LG, Amaral PM. Temperature effects on mechanical behaviour of engineered stones. Constr Build Mater 2011;25:171–4.
[4] Hamoush S, Abu-Lebdeh T, Picornell M, Amer S. Development of sustainable engineered stone cladding for toughness, durability, and energy conservation. Constr Build Mater 2011;25:4006–16.
[5] Vijayalakshmi M, Sekar ASS, Ganesh G. Strength and durability properties of concrete made with granite industry waste. Constr Build Mater 2013;46:1–7.
[6] Bacci D de LC, Landim PMB, Eston SM. Aspectos e impactos ambientais de pedreira em área urbana. Rem Rev Esc Minas 2006;59:47–54.
[7] Li Y, Ren S. Building decorative materials. Elsevier; 2011.
[8] Anovitz LM, Blencoe JG. Dry melting of high albite. Am Mineral 1999;84:1830–42.
[9] Aksay IA, Pask JA. Stable and metastable equilibria in the system SiO_2-Al_2O_3. J Am Ceram Soc 1975;58:507–12.
[10] Maheshwari A, Chawla KK, Michalske TA. Behavior of interface in alumina/glass composite. Mat Sci Eng A-Struct 1989;107:269–76.
[11] Chawla KK, Ferber MK, Xu ZR, Venkatesh R. Interface engineering in alumina/glass composites. Mat Sci Eng A-Struct 1993;162:35–44.
[12] Ringdalen E. Changes in quartz during heating and the possible effects on Si production. JOM 2015;67:484–92.
[13] Silestone® Reference Guide n.d product.silestoneusa.com/pdf/SilestoneReferenceGuide.pdf, Accessed date: September 2016.
[14] A peek at the strength and hardness ratings of granite and marble n.d. granite-marblewa.com/a-peek-at-the-strength-and-hardness-ratings-of-granite-and-marble n.d. (accessed January 30, 2019).
[15] Dekton - Informações técnicas n.d https://www.dekton.com.br/downloads/#documentacionse, Accessed date: 30 January 2019.
[16] Terrazzo. Technical specifications n.d. http://www.euval.com/en/technical-area/terrazzo-technical-specifications, Accessed date: 30 January 2019.
[17] Gomes Ribeiro CE, Sanchez Rodriguez RJ, Carvalho EA. Microstructure and mechanical properties of artificial marble. Constr Build Mater 2017;149:149–55.
[18] Sossai FJM. Technological characterization of decorative stones. Master Thesis Federal University of Viçosa; 2006. (in Portuguese).
[19] Kingery WD, Bowen HK, Uhlmann DR. Introduction to ceramics. second ed. New York: Wiley-Interscience; 1976.
[20] Choi W-K, Kang T-S, Kim N-I, Lee S-J. Study of low-thermal-expansion porcelain employing petalite and β-eucryptite. J Ceram Process Res 2015;16:324–9.
[21] Hsueh CH, Becher PF. Residual thermal stresses in ceramic composites. Part I: ellipsoidal inclusions. Mat Sci Eng A-Struct 1996;212:22–8.
[22] Eshelby JD. The determination of the elastic field of an ellipsoidal inclusion, and related problems. Proc Roy Soc Lond A 1957;241:376–96.
[23] Peitl O, Zanotto ED. Thermal shock properties of chemically toughened borosilicate glass. J Non-Cryst Solids 1999;247:39–49.
[24] Soares VO. Sintering, crystallization, development and characterization of glass-ceramic of low coefficient of thermal expansion of the system Li2O-Al2O3-SiO2 (LAS) PhD Thesis Federal University of São Carlos; 2010 (in Portuguese).
[25] Serbena FC, Soares VO, Peitl O, Pinto H, Muccillo R, Zanotto ED. Internal residual stresses in sintered and commercial low expansion Li_2O–Al_2O_3–SiO_2 glass–ceramics. J Am Ceram Soc 2011;94:1206–14.
[26] Wu T, Zhou J, Wu B. Effect of Y_2O_3 on acid resistance of alumina ceramic. Ceram Int 2017;43:5102–7.
[27] Buchner S, Mikowski A, Lepienski CM, Ferreira EB, Zanotto ED, Torres RD, Soares P. Mechanical and tribological properties of a sintered glass-ceramic compared to granite and porcelainized stoneware. Wear 2011;271:875–80.